Engineered Regeneration 7 (2026) 176–187

Contents lists available at ScienceDirect

Engineered Regeneration

journal homepage: http://www.keaipublishing.com/en/journals/engineered-regeneration/

Asini Corii Colla exhibits anti-photoaging efficacy via activating collagen synthesis and maintaining redox & extracellular matrix homeostasis

Xiao Xie[a,1], Zhijie Chen[a,1], Zesong Zhang[b,1], Zailin Chen[b,1], Cong Li[a], Jianling Zhang[a], Jiahao Yang[c], Zhihui Lu[d], Lei Jia[c], Meimei Fu[e,*], Jinshan Guo[c,e,*]

[a] Liaocheng Key Laboratory of Functional Food Research and Development, Liaocheng Engineering Research Center for Nutrition and Health Consumer Products, Dong'e Ejiao Health Industry Technology Co., Ltd., Liaocheng, 252201, PR China
[b] Department of Endocrinology, Department of Preventive Medicine, Dongguan Qingxi Hospital, Xiangmang Middle Road, Qingxi Town, Dongguan, 523660, PR China
[c] Biomaterials and Stem Cell Research Laboratory, Suzhou Institute of Biomedical Engineering and Technology, Chinese Academy of Science, Suzhou, 215011 PR China
[d] Regenerative Medicine and Tissue Repair Research Center, Huangpu Institute of Materials, 88 Yonglong Avenue of Xinlong Town, Huangpu District, Guangzhou, 511363, PR China
[e] Department of Histology and Embryology, NMPA Key Laboratory for Safety Evaluation of Cosmetics, GDMPA Key Laboratory of Key Technologies for Cosmetics Safety and Efficacy, School of Basic Medical Sciences, Southern Medical University, 1023 Shatai Rd., Guangzhou, 510515, PR China

ARTICLE INFO

Keywords:
Asini Corii Colla
Ultraviolet irradiation
Anti-photoaging
Collagen synthesis

ABSTRACT

Skin photoaging, primarily induced by chronic ultraviolet (UV) irradiation, is characterized by wrinkle formation, skin laxity, and collagen loss. As a traditional Chinese medicine, the potential of Asini Corii Colla (ACO) in protecting against skin photoaging has not been systematically investigated. This study aimed to comprehensively evaluate the anti-photoaging efficacy of ACO and elucidate its underlying mechanisms. Cytotoxicity and *in vitro* bioactivity of ACO were initially assessed in cultured human keratinocytes and dermal fibroblasts, followed by examination of its effects on cell proliferation and migration under normal conditions, and on SA-β-Gal activity, collagen, and elastin synthesis under UV-induced photoaging. Subsequently, a UV-induced skin photoaging mouse model was established to further validate the efficacy *in vivo*. Pathological changes, collagen content, and senescence-related markers in skin tissues were analyzed. *In vitro* results demonstrated that ACO, within a safe concentration range below 20 mg/mL, significantly promoted cell proliferation and migration, inhibited cellular senescence, enhanced collagen synthesis, and suppressed extracellular matrix (ECM) degradation. *In vivo* experiments confirmed that intervention with ACO markedly ameliorated UV-induced photoaging phenotypes in mice, including wrinkle formation and epidermal thickening, while maintaining dermal collagen density and content, and reducing oxidative stress in skin tissue. Collectively, ACO effectively mitigates UV-induced skin photoaging by promoting skin cell repair and regeneration, enhancing collagen synthesis, and maintaining redox homeostasis. These findings provide a solid scientific foundation for its potential application as an anti-photoaging agent.

1. Introduction

The skin serves as the body's primary barrier against environmental damage. Prolonged exposure to ultraviolet (UV) irradiation induces photoaging, which is clinically distinct from intrinsic aging and characterized by deep wrinkles, skin laxity, coarse texture, abnormal pigmentation, and loss of elasticity [1,2]. The pathophysiological mechanisms involve oxidative stress accumulation, ECM degradation, collagen depletion, and accelerated cellular senescence [2]. Recent advances have highlighted the critical roles of specific signaling pathways, including TGF-β/Smad in collagen synthesis, MAPK/AP-1 in MMP regulation, and Nrf2/ARE in antioxidant defense, in the pathogenesis of UV-induced skin photoaging [3–5]. Current interventions, including physical protection, retinoids, antioxidants, and laser therapy, offer limited efficacy and are often associated with adverse effects such as strong irritation, high cost, or suboptimal outcomes [6]. Therefore, the development of safe and effective photoprotective agents derived from natural products represents a major focus in dermatological and cosmetic research [7]. Indeed, accumulating evidence has demonstrated that various natural products, such as plant-derived polyphenols, flavonoids, and bioactive

Peer review under the responsibility of editorial board of Engineered Regeneration.
* Corresponding authors.
E-mail addresses: fmm05037726@163.com (M. Fu), jsguo4127@smu.edu.cn, guojinshan@sibet.ac.cn (J. Guo).
[1] These authors contribute equally.

https://doi.org/10.1016/j.engreg.2026.07.001
Received 9 April 2026; Received in revised form 26 June 2026; Accepted 13 July 2026
Available online 14 July 2026

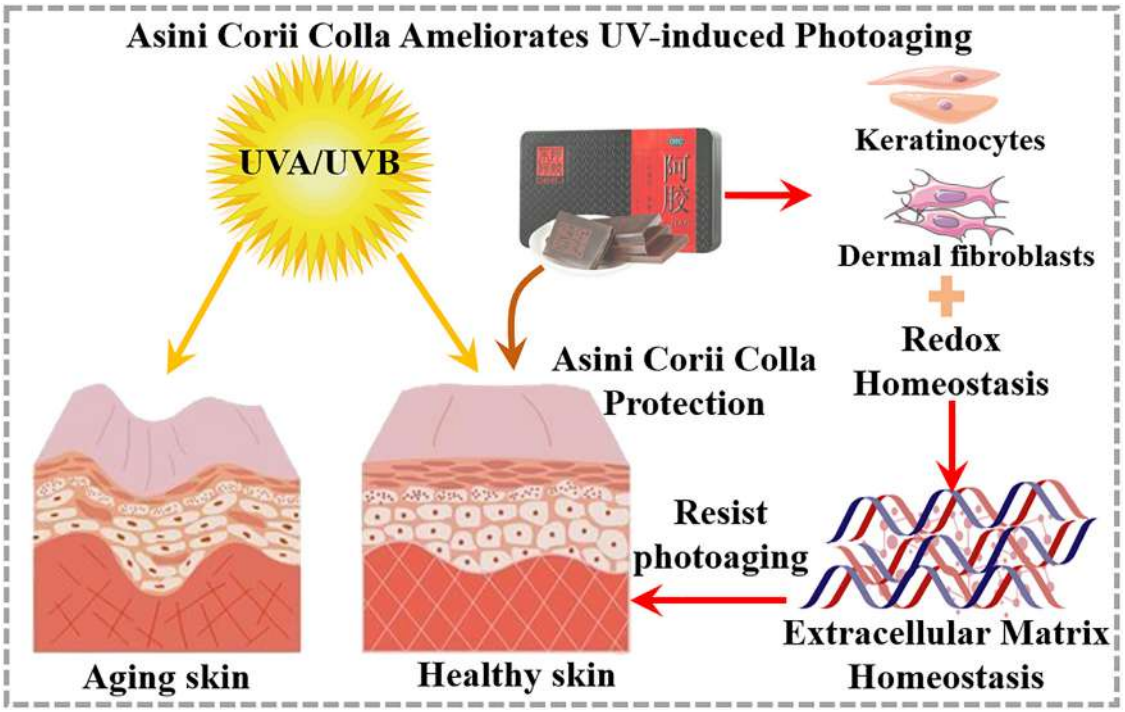

Fig. 1. Proposed mechanism of ACO against UVA/UVB-induced photoaging. The protection is characterized by cytoprotection, restoration of redox and cellular homeostasis, and enhanced ECM integrity, which collectively contribute to the amelioration of photoaging damage.

peptides, exert anti-photoaging effects through multiple mechanisms, including ROS scavenging, MMP inhibition, and collagen synthesis promotion [8,9].

Asini Corii Colla (Ejiao, ACO) is a renowned tonic in the treasure trove of Chinese medicine, derived from donkey hide through traditional boiling techniques [10]. Since ancient times, it has been used to replenish and nourish blood, tonify yin, and moisten dryness [11]. Besides, it is classified as a superior-grade herb in classical literature such as Shennong's Classic of Materia Medica [12]. Modern pharmacological studies have revealed that ACO possesses activities including hematopoiesis promotion, immune enhancement, and anti-fatigue effects [13]. These pharmacological properties are largely attributed to its rich composition of collagen peptides, amino acids, glycosaminoglycan and trace elements [13]. Given the connection between skin health and the traditional Chinese medical concepts of nourishing Qi and blood, along with collagen's role as a key protein in maintaining skin structural integrity and youthfulness, ACO is hypothesized to have therapeutic effects on skin photoaging [14]. To date, only a limited number of studies have explored the dermatological applications of ACO. For instance, Li et al. reported that ACO extracts exhibit anti-skin-aging effects [15], Tie et al. demonstrated the antioxidant activity of E'jiao and Cubilose Formula and its ability to improve collagen expression in human skin fibroblasts during oxidative damage [16], and Chuo et al. systematically evaluated the skin tone-improving efficacy of phenolic compounds from ACO cake, showing that the extracts effectively inhibit tyrosinase activity and reduce melanin production in melanoma cells [17]. However, these investigations have primarily focused on isolated aspects of ACO's activity, whether antioxidant protection, melanin inhibition, or collagen maintenance, without integrating epidermal repair, dermal rejuvenation, and redox balance into a unified mechanistic framework. Systematic scientific research on its anti-photoaging effects remains scarce, and its efficacy and underlying mechanisms require further elucidation [18].

Therefore, this study aims to systematically evaluate the anti-photoaging efficacy of ACO and explore its underlying mechanisms using a combination of *in vitro* cell models and *in vivo* animal experiments. Specifically, we assessed the effects of ACO on key biological processes in primary skin cells (fibroblasts and keratinocytes), including proliferation, migration, senescence, and collagen synthesis. Furthermore, a UV-induced mouse model of photoaging was established to validate the protective effects of ACO on skin structure and function at the histopathological level. This is the first study to comprehensively characterize the anti-photoaging effects of ACO, which are associated with improvements in epidermal repair, dermal rejuvenation, and redox balance. This research provides robust scientific evidence to support the advanced development and clinical application of ACO, and opens new avenues for the application of natural medicines in skin care (Fig. 1).

2. Experimental

2.1. Materials

ACO powder (Batch no: 20240802) was obtained from Dong'e Ejiao Health Industry Technology Co., Ltd. (Liaocheng, China). Trypsin (sequencing grade) was purchased from Promega Corporation (Madison, WI, USA). Acetonitrile (MS grade) and formic acid (MS grade) were obtained from Macklin Biochemical Co., Ltd. (Shanghai, China). Ammonium bicarbonate (guaranteed reagent) was sourced from Sinopharm Chemical Reagent Co., Ltd. (Shanghai, China). Trichloroacetic acid (analytical grade) and acetone (analytical grade) were procured from Aladdin Reagent Co., Ltd. (Shanghai, China). The reference standard of Asini Corii Colla was provided by Beijian Testing Technology Co., Ltd., complying with the Chinese Pharmacopoeia (2015 edition) standards. Dulbecco's Modified Eagle Medium (DMEM), Fetal Bovine Serum (FBS), trypsin, and penicillin-streptomycin (dual-antibiotic solution) were purchased from Gibco (USA). Phosphate-Buffered Saline (PBS) was sourced from Beijing Psaitong Biotechnology Co., Ltd (Beijing, China). Vitamin E (VE) was procured from Shanghai Acmec Biochemical Technology Co. Ltd (Shanghai, China). The Cell Counting Kit-8 (CCK-8) and Acridine Orange/Ethidium Bromide (AO/EB) double fluorescent staining kit were obtained from Abbkine (Wuhan, China). Assay kits for hydroxyproline (HYP), superoxide dismutase (SOD), and malondialdehyde (MDA) were

provided by the Nanjing Jiancheng Bioengineering Institute (Nanjing, China). ELISA kits for type I collagen (Col-I), type III collagen (Col-III), Elastin (ELN), and Matrix Metalloproteinase-1 (MMP-1) were purchased from Bioswamp Life Science Lab (Wuhan, China). The BCA Protein Assay Kit was obtained from Beyotime Biotechnology Co., Ltd. (Beijing, China). The human immortalized keratinocyte cell line (HaCaT) was obtained from Cellverse Co., Ltd. (Shanghai, China) with catalog number iCell-h066 in [2024/12], and the Research Resource Identifier (RRID) is [RRID: CVCL_0038]. The human skin fibroblast (HSF) cell line was obtained from Cellverse Co., Ltd. (Shanghai, China) with catalog number iCell-0051a in [2024/12], and the Research Resource Identifier (RRID) is [RRID: CVCL_D003].

2.2. LC-MS/MS analysis of donkey-derived signature peptides and amino acids in ACO

Following previously reported methods [19], LC-MS/MS (Liquid Chromatography–Tandem Mass Spectrometry) analysis of ACO was performed as described below. Frozen ACO (8 mg) was dissolved and diluted to 2 mL with ultrapure water. An equal volume of 30% trichloroacetic acid solution was slowly added, and the mixture was vortexed and incubated at 4 ˚C for 20 min. The sample was then centrifuged at 7000 × g for 5 min, and the supernatant was discarded. The precipitate was washed twice with 2 mL of ice-cold acetone, followed by centrifugation and removal of the supernatant. The resulting pellet was dissolved in 10-20 mL of 1% (w/v) ammonium bicarbonate solution with the aid of ultrasonication to obtain the ACO extract. The extract was filtered through a 0.22-μm membrane, and 400 μL of the filtrate was mixed with 40 μL of trypsin solution (1 mg/mL), followed by incubation at 37˚C for 16 h for enzymatic digestion. A reference standard of ACO was processed in parallel following the same procedure. For protein quantification, an appropriate amount of ACO sample was subjected to the BCA assay, using bovine serum albumin as the standard to generate a calibration curve.

LC-MS/MS analysis was performed on a TSQ Altis triple-quadrupole mass spectrometer coupled to a liquid chromatography system (Thermo Fisher Scientific). Chromatographic separation was achieved on a Waters ACQUITY UPLC BEH C_{18} column (50 mm × 2.1 mm, 1.7 μm) at a flow rate of 0.3 mL/min and a column temperature of 30 ˚C. The mobile phase consisted of 0.1% formic acid in water (A) and 0.1% formic acid in acetonitrile (B). The gradient elution program was set as follows: 0-1.0 min, 5% B; 1.0-4.5 min, linear increase to 30% B; 5.6-6.6 min, increase to 95% B; 6.7 min, return to 5% B and equilibrate until 8.0 min. The injection volume was 5 μL. Mass spectrometry was conducted in electrospray positive-ion mode (ESI^+) with multiple reaction monitoring (MRM). The spray voltage was set to 3500 V, and the ion transfer tube temperature was maintained at 300 ˚C. The donkey-derived signature peptides A1 and A2 were identified by comparing their retention times and precursor ion masses with those of the reference standard, with a retention time deviation tolerance of ±2.5%. The signal-to-noise ratio of the MRM chromatographic peaks was required to be greater than 3:1. For qualitative identification of amino acids and small nitrogen-containing compounds, the MS data were processed using the mass spectrometry software against the PCDL database with the FBF (Fragment-Based Finding) algorithm. Quantification was performed using the external standard method, with calibration curves constructed from the standard working solutions. All samples were analyzed in triplicate, and the results were expressed as mean values.

2.3. In Vitro *cell experiments*

The HaCaT and HSF were cultured in DMEM supplemented with 10% (v/v) fetal bovine serum (FBS) and 1% (v/v) penicillin-streptomycin at 37 ˚C in a humidified atmosphere of 5% CO_2.

To prepare the extract, 1 g ACO powder was dissolved in 2 mL of ultrapure water and filter-sterilized through a 0.22 μm membrane to obtain a 500 mg/mL stock solution. This stock solution was subsequently subjected to serial dilution to generate a concentration gradient of 0.156, 0.312, 0.625, 1.25, 2.5, 5, 10, and 20 mg/mL. This concentration range was selected to cover sub-cytotoxic doses while capturing the dose-dependent effects of ACO on cell proliferation, migration, and senescence *in vitro*.

2.3.1. Cytotoxicity assay

HaCaT cells were seeded in a 96-well plate at a density of 1×10^4 cells per well (100 μL per well) and cultured for 24 h. After incubation, the culture medium was replaced with a pre-mixed medium containing various concentrations of ACO, with five replicate wells per concentration. Following another 24-hour incubation, a CCK-8 working solution was prepared by mixing CCK-8 reagent with fresh medium at a 1:10 ratio. Then, 100 μL of the CCK-8 working solution was added to each well. After 30 min of incubation, the absorbance at 450 nm was measured using a microplate reader, and cell viability was calculated accordingly.

2.3.2. Cell proliferation assay

HaCaT cells were seeded in a 24-well plate with a density of 5000 cells/well and incubated for 24 h. The culture medium was then replaced with complete medium (containing 10% (v/v) FBS and 1% (v/v) penicillin-streptomycin) supplemented with ACO solution. Cells cultured in the pure complete medium without ACO served as the control group. After 1, 3, and 5 d of further incubation, cell viability was assessed using the CCK-8 assay and AO/EB staining, respectively [20].

2.3.3. Cell scratch assay

A monolayer of HaCaT cells was cultured in a 24-well plate until reaching 100% confluency. A uniform scratch was then made in each well using a sterile 1000 μL pipette tip. The detached cells were gently removed by washing twice with PBS. Subsequently, the cells were treated with ACO containing complete medium (containing 2% FBS). The cell migration was monitored, and images were captured under an inverted fluorescence microscope (Olympus CKX41, Tokyo, Japan) at 0, 24, and 48 h post-scratching [21].

2.3.4. Assessment of cellular senescence

HSF cells were seeded in 24-well and 96-well plates with cell densities of 10000 and 5000 cells/well, respectively. Upon reaching complete confluence, cells were cultured for 24 h in complete medium supplemented with either ACO solution or VE (0.05%) as a positive control. VE was selected as the positive control due to its well-established antioxidant properties and its extensive use as a reference compound in anti-photoaging and anti-senescence studies [22,23]. Following this pretreatment, the medium was discarded and replaced with PBS to cover the cells during irradiation. Cells were then exposed to UVA (1.6 J/cm^2) and UVB (0.4 J/cm^2) irradiation, with the output intensity calibrated using a UV radiometer prior to each exposure. After irradiation, the PBS was aspirated and immediately replaced with fresh complete medium containing the corresponding concentrations of ACO or VE, and cells were cultured for an additional 24 h before further analysis. Following treatment, cell viability was assessed in 96-well plates using the CCK-8 assay. Concurrently, cells in 24-well plates were subjected to SA-β-Gal staining kit per the manufacturer's instructions, with the percentage of SA-β-Gal-positive cells quantified using ImageJ software. The concentrations of Col-I, Col-III, ELN, and MMP-1 in the cell culture supernatants were quantified using commercial ELISA kits, strictly according to the manufacturers' protocols.

2.4. In Vivo *experiments in a mouse model*

2.4.1. Establishment of the Mouse Photoaging Model and Evaluation of Photoaging in Mice

Male Kunming mice (6 weeks old, weighing 20-25 g) were purchased from Guangzhou Yancheng Biotechnology Co., Ltd. All animal experiments were conducted in compliance with the Animal Experimental

Committee of Institute of Biological and Medical Engineering, Guangdong Academy of Sciences (Approval *No.*K2024-01-272-472), which complies with the Chinese Guidelines for the Ethical Use of Animals in Experimental Research and the ARRIVE (Animal Research: Reporting of *In Vivo* Experiments) guidelines. All animals were housed in a specific pathogen-free (SPF) facility under controlled conditions: temperature at (24 ± 2) ˚C, relative humidity of 30%-70%, and a 12 h light/12 h dark cycle. Mice had ad libitum access to standard laboratory chow and autoclaved water, and were maintained at a maximum of five per cage. Following a 1-week acclimatization period, the dorsal hair of each mouse was removed using a depilatory cream. The skin was examined daily to ensure the depilated area remained intact, and only mice with unblemished skin were included in subsequent experiments. The mice were randomly assigned to six groups (n = 10 per group): Blank group (depilation only, no further treatment), Control group (application of deionized water followed by UV irradiation), RHT-III group (Recombinant humanized type III collagen, application of 20 mg/mL Recombinant humanized type III collagen solution, followed by UV irradiation), and ACO low-, medium-, and high-dose groups (application of 10, 20, and 40 mg/mL ACO solution, respectively, followed by UV irradiation). RHT-III used in this study is provided by Prof. Sheng Xiong of Jinan University, the provider confirmed that the RHT-III (AnaGF® rDuCol) was originally obtained from Guangzhou Cheer-Derm Biotech Co Ltd, No: QD-A-250526-01. RHT-III was selected as the positive control because exogenous collagen supplementation is a well-established strategy for combating skin aging, and it serves as a clinically relevant reference to evaluate whether the anti-photoaging efficacy of ACO is comparable to that of existing collagen-based products [24,25]. It should be noted that higher concentrations (10-40 mg/mL) were selected for topical administration to overcome the skin barrier, comprising the stratum corneum, epidermis, and dermis, which significantly restricts the transdermal absorption of macromolecules such as collagen peptides. For daily administration, 200 μL of the corresponding solution was topically applied to the depilated dorsal skin of each mouse. Following application, the mice were kept in the dark for 1 h to allow sufficient percutaneous absorption. After preheating and stabilization of UVA and UVB lamps, the depilated dorsal skin was exposed to UV irradiation at a dose of 1.6 J/cm^2 for UVA and 0.4 J/cm^2 for UVB (total daily dose of 2 J/cm^2). The UV treatment was performed five times per week for a total of 8 consecutive weeks. Routine observations and documentation of dorsal skin changes were performed throughout the experimental period.

2.4.2. Histological analysis of photoaging in mice

At the endpoint of the photoaging experiment, mice were euthanized, and a segment of dorsal skin was harvested. Tissue samples were fixed in 4% Paraformaldehyde, paraffin-embedded, and sectioned into 4-μm-thick slices using a microtome. These sections were subsequently stained with hematoxylin and eosin (H&E), Masson's trichrome, and Verhoeff's Van Gieson (EVG) to assess histological alterations associated with photoaging. Additionally, another portion of the dorsal skin was homogenized, and levels of HYP, SOD, and MDA were quantified according to the respective commercial kits' instructions to further evaluate collagen loss and oxidative stress status.

2.5. Statistical analysis

All experiments were performed with at least three independent biological replicates. Data are presented as mean ± standard deviation (SD), unless otherwise specified. Statistical analyses were performed using GraphPad Prism 9.0 (GraphPad Software, USA). For comparisons between two groups, a two-tailed Student's t-test was used. For comparisons among three or more groups, one-way analysis of variance (ANOVA) was performed, followed by Tukey's post hoc test for multiple comparisons. Results with $p < 0.05$ were deemed statistically significant. *, **, and *** denote $p < 0.05$, $p < 0.01$, and $p < 0.001$, respectively.

3. Results and discussion

3.1. LC-MS/MS identification of donkey-derived signature peptides and amino acids in Asini Corii Colla

The total protein content of untreated ACO samples was determined to be 47.8% by the BCA assay, indicating that protein constitutes a major component of the sample (the standard curve is shown in **Fig. S1**). The amino acids and small nitrogen-containing compounds in the ACO sample were analyzed by LC-MS/MS, and the total ion current chromatogram is presented in **Fig. S2**. Through comparison with the PCDL database and identification using the FBF (Fragment-Based Finding) algorithm, a total of 17 amino acids and small nitrogen-containing compounds were detected in the sample (**Fig. S3**), including hydroxyproline, glycine, proline, phenylalanine, glutamate, cysteine, norleucine, valine, histidine, serine, aspartic acid, pipecolic acid, pyroglutamic acid, tryptophan, arginine, dehydroamino-x-butyric acid, and hydroxylysine. Among these, hydroxyproline is a characteristic amino acid of collagen [26], while glycine and proline are its major constituent amino acids; the detection of these three amino acids indicates that the sample possesses collagen-like compositional features. The match scores of all identified compounds ranged from 69.49 to 99.97, with 16 compounds scoring above 85, demonstrating high confidence in the identification results. The detailed identification results are provided in **Table S1**.

The donkey-derived signature peptides A1 and A2 were detected using multiple reaction monitoring (MRM) mode, and their secondary chromatograms, full-scan mass spectra, and MS/MS spectra are shown in **Fig. S4**. The results showed that signature peptide A1 (retention time: 19.326 min, Mass 936.5062) and peptide A2 (retention time: 22.616 min, Mass 1234.5989) were both detected in the sample, with MRM chromatographic peak signal-to-noise ratios greater than 3:1. The donkey-derived origin of the sample was confirmed by comparison of retention times (deviation ≤ 2.5%) and precursor ion masses with those of the signature peptide reference standards. The detailed mass spectrometric identification parameters for the donkey-derived signature peptides are provided in **Table S2**.

3.2. Cytotoxicity assay of ACO

Keratinocytes, as the primary cell type in the epidermal layer of the skin, serve as the first line of defense against UV irradiation and are also the main target cells for UV-induced effects on the skin [27]. This study first utilized HaCaT to evaluate the biocompatibility of ACO. As shown in Fig. 2A, cytotoxicity test results indicate that within the concentration range of 0.156-20 mg/mL, ACO treatment groups exerted no significant cytotoxic effects on cells. Cell viabilities remained above 100% in all experimental groups, demonstrating that ACO exhibits good biosafety within this concentration range.

3.3. Effect of ACO on cell proliferation

To investigate the long-term effects of ACO on keratinocytes, we continuously monitored cell proliferation. As shown in Fig. 2B and 2C, all the treatment groups exhibited higher proliferation rates than the control group (405.87%). None of the ACO treatment groups exhibited cytotoxicity, and all concentrations significantly promoted the proliferation of HaCaT cells. Among all tested concentrations, the ACO-2.5 group demonstrated the most pronounced pro-proliferative effect, achieving a cell proliferation rate of 440.27% (with the cell amount of the control group on day 1 as 100%) on day 5 (Fig. 2C). This was followed by the ACO-0.625 group (426.63%), and even at the lowest concentration, ACO-0.156 also exerted a slight proliferation promotion effect (412.26%). Statistical analysis revealed significant differences between the ACO-2.5 and ACO-0.625 groups compared with the control group ($p < 0.01$). These results indicate that ACO possesses a remarkable ability to promote cell proliferation within the tested concentration range, and

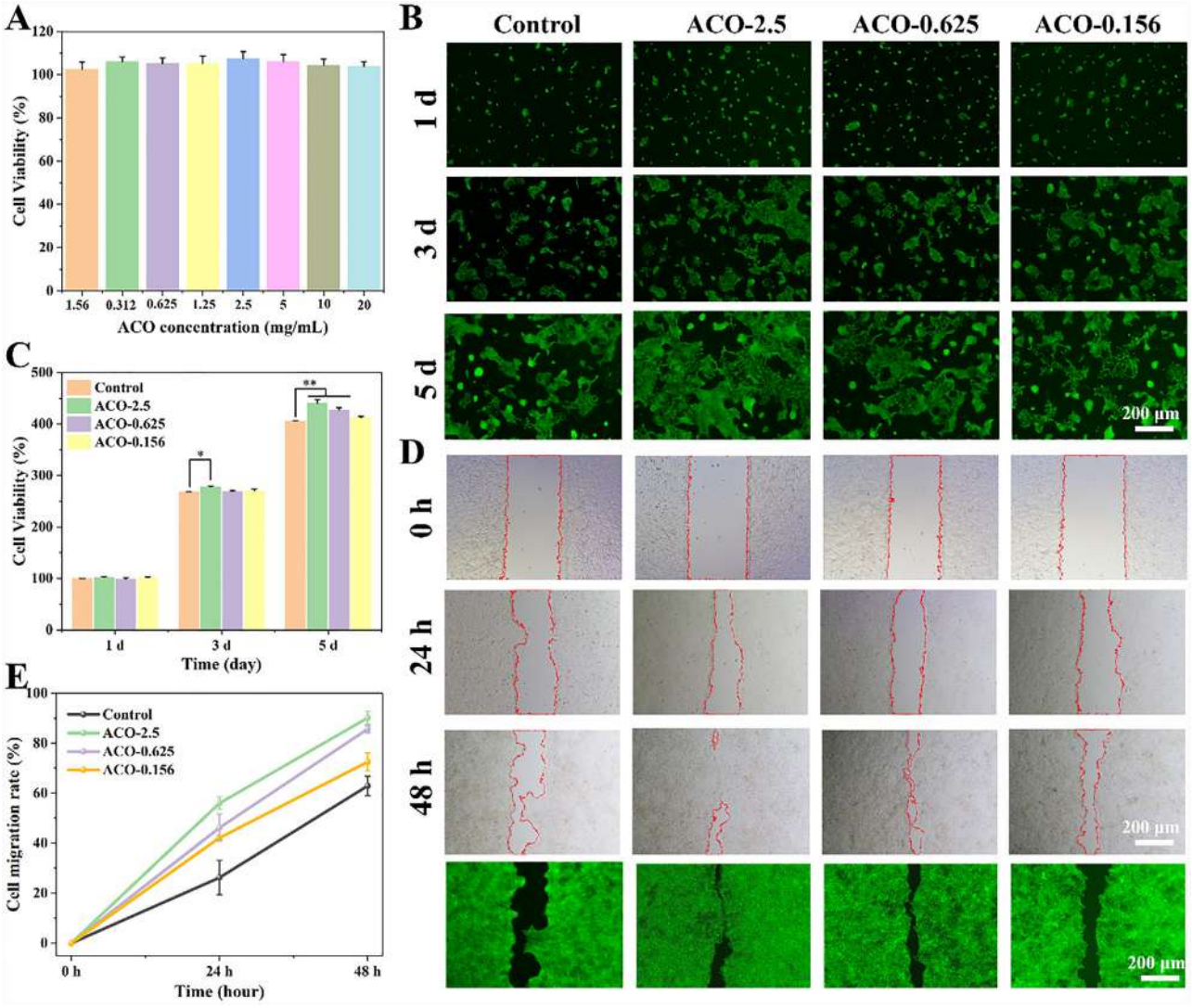

Fig. 2. Effects of ACO on keratinocytes. (A) Cytotoxicity of ACO on HaCaT cells (n = 5). (B) Representative Live/Dead staining images of HaCaT cells treated with ACO for 1, 3, and 5 d. (C) Viability of HaCaT cells following ACO treatment at 1, 3, and 5 days (n = 5). (D) Scratch wound healing assay images of HaCaT cells cultured with ACO for 0, 24, and 48 h. (E) Calculated cell migration rates across different treatment groups (n = 5). $^{*}p < 0.05$, $^{**}p < 0.01$, $^{***}p < 0.001$.

this pro-proliferative effect displayed a certain concentration-dependent trend within the tested range.

3.4. Effect of ACO on cell migration

To evaluate the effect of ACO on cell migration, a scratch assay was performed, which is a widely used method for assessing cell migration and repair capacity [28]. As shown in Fig. 2D and 2E, significant differences in cell migration rates were observed between all ACO-treated groups and the control group ($p < 0.05$). The migration rates in the ACO groups were markedly higher than those in the control group. Specifically, after 48 h, the cell migration rates in the ACO-2.5 and ACO-0.625 groups reached 90.19% and 85.72%, respectively (Fig. 2E). Even at the lowest concentration, ACO-0.156 achieved a migration rate of 72.55%, which was substantially higher than the 63.01% observed in the control group. These results demonstrate that ACO effectively enhances cell migration capacity.

3.5. Effect of ACO on cellular senescence

UV irradiation and other stimuli trigger dermal fibroblast senescence, leading to an imbalance in ECM metabolism. This process promotes the secretion of multiple matrix-degrading enzymes and inhibits collagen synthesis, thereby contributing to the progressive degradation of the skin's dermal structure [29]. To establish a cellular senescence model, cells were pretreated with ACO solution or VE for 24 h, followed by exposure to UVA (1.6 J/cm^2) and UVB (0.4 J/cm^2) irradiation. As shown in Fig. 3A, cell viability assays performed on UV-irradiated cells showed that UV exposure significantly reduced the viability of HSF, with cell viability dropping to only 71.88% of that in the blank control group ($p < 0.001$). In contrast, all ACO pretreatment groups maintained cell viability above 78.20%. The positive control group treated with VE exhibited 96.26% viability, which was not statistically different from the 92.84% viability observed in the ACO-2.5 group. These results indicate that ACO at higher concentrations effectively protects against UV-induced oxidative damage and helps maintain cell viability.

The mechanism of UV-induced cellular senescence involves multiple signaling pathways, including DNA damage, oxidative stress, and telomere dysfunction [30]. UV irradiation triggers the generation of reactive oxygen species (ROS), which in turn causes oxidative damage to cellular macromolecules and activates the DNA damage response, ultimately leading to the establishment of a senescent phenotype [31]. Senescent cells typically display enlarged morphology and high expression of SA-β-Gal, which is active at pH 6.0 [32]. In this study, SA-β-Gal

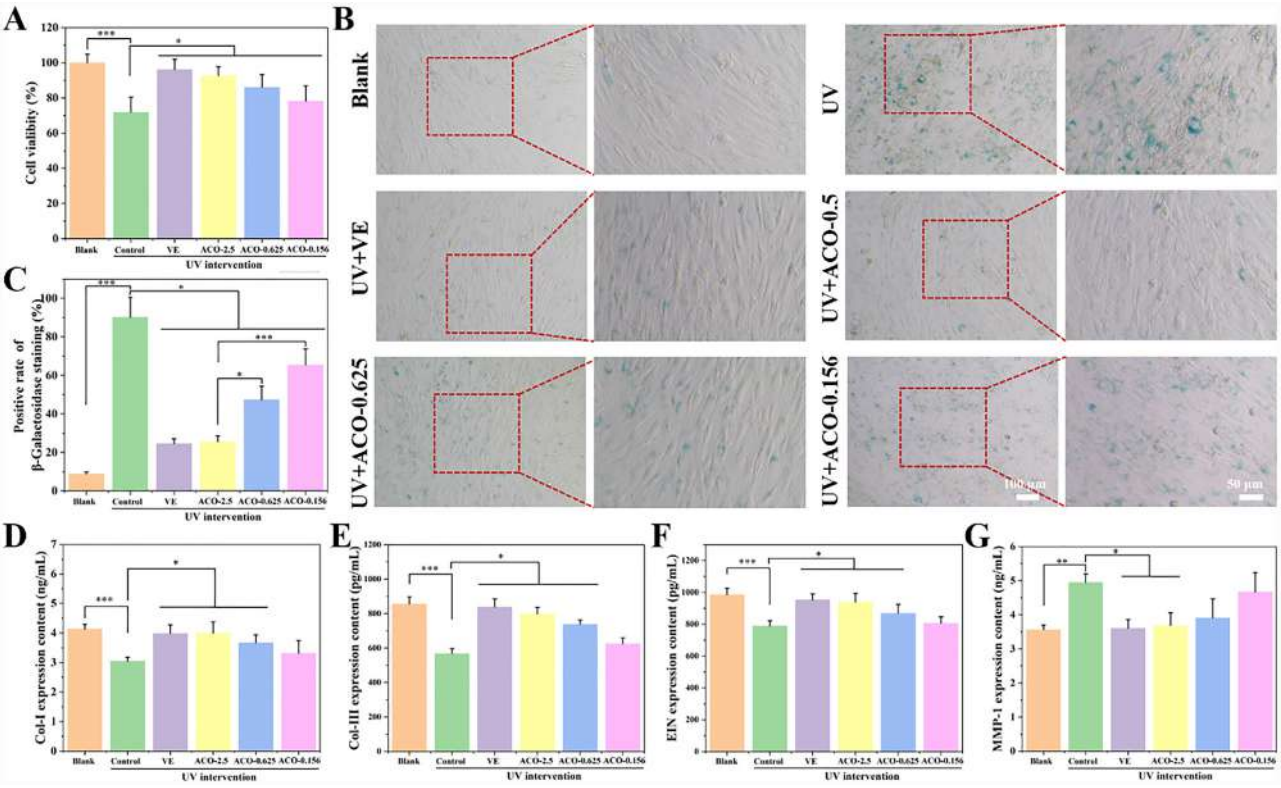

Fig. 3. Effects of ACO on UV-induced senescence in dermal fibroblasts. (A) Cell viability of UV-induced senescent dermal fibroblasts (n = 5). (B) Representative β-galactosidase staining results of UV-induced senescent dermal fibroblasts. (C) Positive rate of β-galactosidase staining in UV-induced senescent dermal fibroblasts (n = 5). ELISA detection of Col-I (D), Col-III (E), ELN (F), and MMP-1 (G) levels in the supernatant of ACO-pretreated cells (n = 5). $^{*}p < 0.05$, $^{**}p < 0.01$, $^{***}p < 0.001$.

activity was measured to evaluate the effect of ACO on UV-induced cellular senescence. As shown in Fig. 3B and 3C, the SA-β-Gal positivity rate in the UV-irradiated model group reached 91.54%, significantly higher than that in the blank control group (8.82%, $p < 0.001$). All ACO treatment groups significantly reduced the SA-β-Gal positive rate in a concentration-dependent manner. Specifically, the SA-β-Gal positive rate in the ACO-2.5 group decreased to 25.59%, which was comparable to that in the VE group (24.53%). The other ACO treatment groups (ACO-0.625 and ACO-1.25) exhibited percentages of 47.38% and 65.43%, respectively, both significantly lower than that of the model control group ($p < 0.05$). These results demonstrate that ACO effectively suppresses UV-induced cellular senescence and exhibits significant anti-senescence activity.

3.6. Effect of ACO on the expression of key ECM components and degrading enzymes

Cellular senescence disrupts ECM homeostasis, leading to dysregulated expression of key structural components (such as collagen and elastin) and their degrading enzymes (including MMPs) [33]. To investigate the effect of ACO on the expression of key ECM components and their degrading enzymes in the context of UV-induced senescence, we quantified the levels of collagens, elastin, and MMPs. Col-I serves as a fundamental structural component for maintaining dermal strength and skin firmness, and its reduced expression is a primary cause of skin laxity and wrinkle formation [34]. As shown in Fig. 3D, the expression of Col-I was significantly decreased in the UV-induced senescence model group. Compared with the blank group (4.13 ng/mL), the model control group exhibited a markedly lower level of only 3.04 ng/mL, and this difference was statistically significant ($p < 0.001$). In contrast, both VE and all concentrations of ACO effectively inhibited this downward trend. Specifically, the expression level in the VE group was 3.98 ng/mL, while that in the ACO-2.5 group was 4.01 ng/mL, with no statistically significant difference observed between the two groups. This indicates that higher concentrations of ACO exert a capacity to promote Col-I expression comparable to that of VE. Col-III forms a fine elastic fiber network that works synergistically with Col-I to support dermal structure, playing an indispensable role in maintaining skin firmness and flexibility [35]. As shown in Fig. 3E, UV exposure significantly reduced the level of Col-III in cells. Compared with the blank group (856.18 pg/mL), the Col-III level in the model control group was only 568.06 pg/mL, with a statistically significant difference observed ($p < 0.001$). In contrast, VE and all ACO treatment groups effectively reversed this decline and promoted Col-III expression to varying degrees.

The elastic network formed by elastin serves as the molecular basis for skin's ability to rebound after stretching, and its degradation directly leads to skin laxity and contour alterations [36]. Analysis of cellular elastin expression levels (Fig. 3F) revealed that, compared with the blank group, the model control group exhibited a significant reduction in elastin expression. In contrast, the elastin expression levels in the VE group and the different concentration groups of ACO (ACO-2.5, ACO-0.625, ACO-0.156) were 952.89, 939.23, 869.38, and 806.38 pg/mL, respectively, all of which were higher than that of the model control group (789.46 pg/mL). These results indicate that the suppression of UV-induced oxidative stress may contribute to the enhancement of elastin secretion, and indirectly suggest that ACO may exert its protective effects through the inhibition of oxidative stress pathways. MMP-1 is a key enzyme responsible for initiating the degradation of Col-I in the dermal structure, and its overactivation is a critical factor leading to collagen loss, dermal collapse, and wrinkle formation [37]. As shown in Fig. 3G, the MMP-1 expression level in the VE group was the lowest (3.60 ng/mL), indicating that antioxidant intervention can effectively inhibit collagen degradation. The MMP-1 expression in the ACO-2.5 group was 3.68 ng/mL, significantly lower than that in the model control group

(4.94 ng/mL, $p < 0.001$), and comparable to that of the blank group without UV treatment (3.56 ng/mL). These results demonstrate that treatment with a higher concentration of ACO can downregulate MMP-1 expression during UV-induced senescence, thereby indirectly reducing collagen degradation.

3.7. Evaluation of the anti-photoaging effect of ACO in mice

Based on the potential of ACO to inhibit skin photoaging and delay cellular senescence revealed by *in vitro* experiments, this study further established a mouse photoaging model to verify its ameliorative effect on UV-induced skin damage (Fig. 4A). The mice were anesthetized and placed under a UVA/UVB combined UV lamp to establish the photoaging model, and the irradiation intensity was monitored and recorded (Fig. 4B). After 4 weeks of modeling, the model control group showed varying degrees of desquamation, wrinkling, and other pathological changes on the dorsal skin. In contrast, the ACO treatment groups (ACO-10, ACO-20, and ACO-40) exhibited gradually reduced severity of skin damage, demonstrating a dose-dependent improvement trend (Fig. 4C). The skin condition of the positive control group (RHT- III) group was generally similar to that of the ACO-20 group. Following 8 weeks of continuous intervention, the dorsal skin damage in the model control group further worsened, presenting with numerous deep wrinkles, pinpoint-sized erythema, pigmentation, skin roughness and thickening, laxity, and significantly reduced elasticity. As the concentration of ACO increased, the skin condition of the mice improved significantly: the ACO-10 group showed numerous shallow wrinkles, a few deep wrinkles, skin thinning, mild erythema, and pigmentation; the ACO-20 and RHT-III groups displayed only a few shallow wrinkles; while the ACO-40 group exhibited the mildest photoaging with a relatively smooth and even skin surface, exhibiting the optimal improvement effect (Fig. 4C).

According to the established skin photoaging assessment criteria [38], we conducted macroscopic scoring on the dorsal skin of the mice (Fig. 4D). With the UV-untreated normal mouse skin as the baseline (score = 0), the results showed that the untreated UV-irradiated group (model control group) achieved a score of 5.33. The three ACO intervention groups (ACO-10, ACO-20, and ACO-40) achieved scores of 4.00, 3.00, and 2.66, respectively, demonstrating a dose-dependent improvement trend. The RHT-III positive control group scored 3.33 (Fig. 4E).

According to the skin elasticity assessment protocol, the dorsal skin of ether-anesthetized mice was gently pinched along the midline between the thumb and index finger and lifted until the hind limbs just touched the desktop. The skin was held for 10 seconds, then released, and the time required for the skin to return to its original state was recorded (Fig. 4F). The results showed that the skin recovery time was significantly prolonged in the model control group (34.66 s), exhibiting a statistically significant difference compared with the blank group ($p < 0.001$). As the concentration of ACO increased, the negative impact of UV irradiation on skin elasticity was markedly attenuated, and the skin recovery time in all ACO treatment groups was shortened to less than 28 s. Specifically, the effect in the RHT-III group (19.66 s) was similar to that in the ACO-20 group (19.66 s), while the skin recovery time in the ACO-40 group was further reduced to 18 s, exhibiting no statistically significant difference from the blank group (Fig. 4F).

3.8. Histological analysis of ACO on photoaging mice

To evaluate the ameliorative effect of ACO on photoaged mouse skin, skin tissue samples collected after 8 weeks of intervention were subjected to H&E staining (Fig. 5A), Masson's trichrome staining (Fig. 5B), and EVG staining (Fig. 5C). As shown in Fig. 5A, the dorsal skin of the normal blank group exhibited an intact structure with a well-defined epidermal layer consisting of approximately 1-2 layers of neatly arranged keratinocytes. The dermis contained abundant fibrous tissue with uniform distribution and a continuous structure, without significant disruption or disorganization, and the epidermal thickness was measured at 25.00 μm (Fig. 5D). Compared with the blank group, the UV-irradiated untreated group (model control group) displayed a significantly thickened epidermis, comprising approximately 8-12 layers of keratinocytes with indistinct cellular stratification (Fig. 5A). The dermal fibers were decreased in quantity and loosely arranged, with extensive inflammatory cell infiltration throughout the entire dermal layer, and the epidermal thickness reached 96.81 μm (Fig. 5D). The ACO-10 group showed reduced epidermal thickness compared with the model control group (approximately 7-10 layers of keratinocytes, Fig. 5A). The dermal fibers exhibited degeneration and disorganized arrangement, accompanied by mild inflammatory cell infiltration in the superficial to middle dermis. The tissue damage was less severe than that in the model control group, with an epidermal thickness of 70.11 μm (Fig. 5D). In addition, the ACO-20 group demonstrated further thinning of the epidermal layer (approximately 5-8 layers of keratinocytes, Fig. 5A), while dermal fiber degeneration and disorganization persisted, inflammatory cell infiltration was minimal in the superficial dermis. The extent of damage was milder than that in both the model control group and the ACO-10 group, with an epidermal thickness of 45.71 μm (Fig. 5D). Furthermore, the ACO-40 group exhibited the thinnest epidermis among all treatment groups with approximately 3-5 layers of keratinocytes (Fig. 5A). The dermal fibers were more densely arranged than in the previous groups, with only scattered inflammatory cell infiltration in the superficial dermis. Tissue damage was the mildest overall, with an epidermal thickness of 31.99 μm (Fig. 5D). Additionally, the RHT-III group showed effects similar to those of the ACO-20 group, with an epidermal layer comprising approximately 5-8 layers of keratinocytes (Fig. 5A). Dermal fibers displayed degeneration and disarray with minimal inflammatory cell infiltration in the superficial dermis, and the damage was less severe than that in the model control group and the ACO-10 group, with an epidermal thickness of 36.12 μm (Fig. 5D).

In Masson's trichrome staining results (Fig. 5B), the dermal collagen fibers in the normal blank group displayed a regular wavy morphology with uniform distribution. Compared with the blank group, the model control group exhibited marked degradation, degeneration, and fragmentation of collagen fibers. In contrast, the three ACO treatment groups (ACO-10, ACO-20, and ACO-40) showed denser arrangement and statistically significantly increased content of dermal collagen fibers relative to the model control group. Among these, the ACO-40 group demonstrated the most prominent effect, characterized by the highest collagen density, tightly packed and orderly arranged fibers, and even distribution throughout the dermis. HYP accounts for approximately 13.4% of the collagen content, and its measurement in skin tissue is therefore often used as a key indicator for screening anti-aging agents [39]. Compared with the blank group (2.40 μg/mL), the HYP content in the skin of the model control group was statistically significantly reduced to 1.92 μg/mL (Fig. 5E). In contrast, the HYP levels in the RHT-III group and various concentrations of ACO groups (ACO-10, ACO-20, and ACO-40) were 2.22, 2.14, 2.23, and 2.30 μg/mL, respectively, all of which were statistically significantly higher than those in the model control group. Consistent with the Masson's trichrome staining results, these findings indicate that ACO treatment can effectively mitigate the adverse effects of UV irradiation on skin collagen and inhibit its degradation.

EVG staining is a commonly used histological method for distinguishing black elastic fibers from red collagen fibers [40]. In the normal blank group, the elastic fibers in mouse skin exhibited a clear structure, slight waviness, and uniform distribution, without observable breakage or fragmentation (Fig. 5C). In contrast, the model control group showed disorganized arrangement of elastic fibers, characterized by thickening, fragmentation, curling, and tangling. Compared with the model control group, the RHT-III and three ACO concentration groups (ACO-10, ACO-20, ACO-40) demonstrated significant improvements in the overall structure of elastic fibers, with markedly reduced breakage and degeneration. Most fibers displayed normal morphology, clear structure, and slight curvature. As the concentration of ACO increased, the morphology

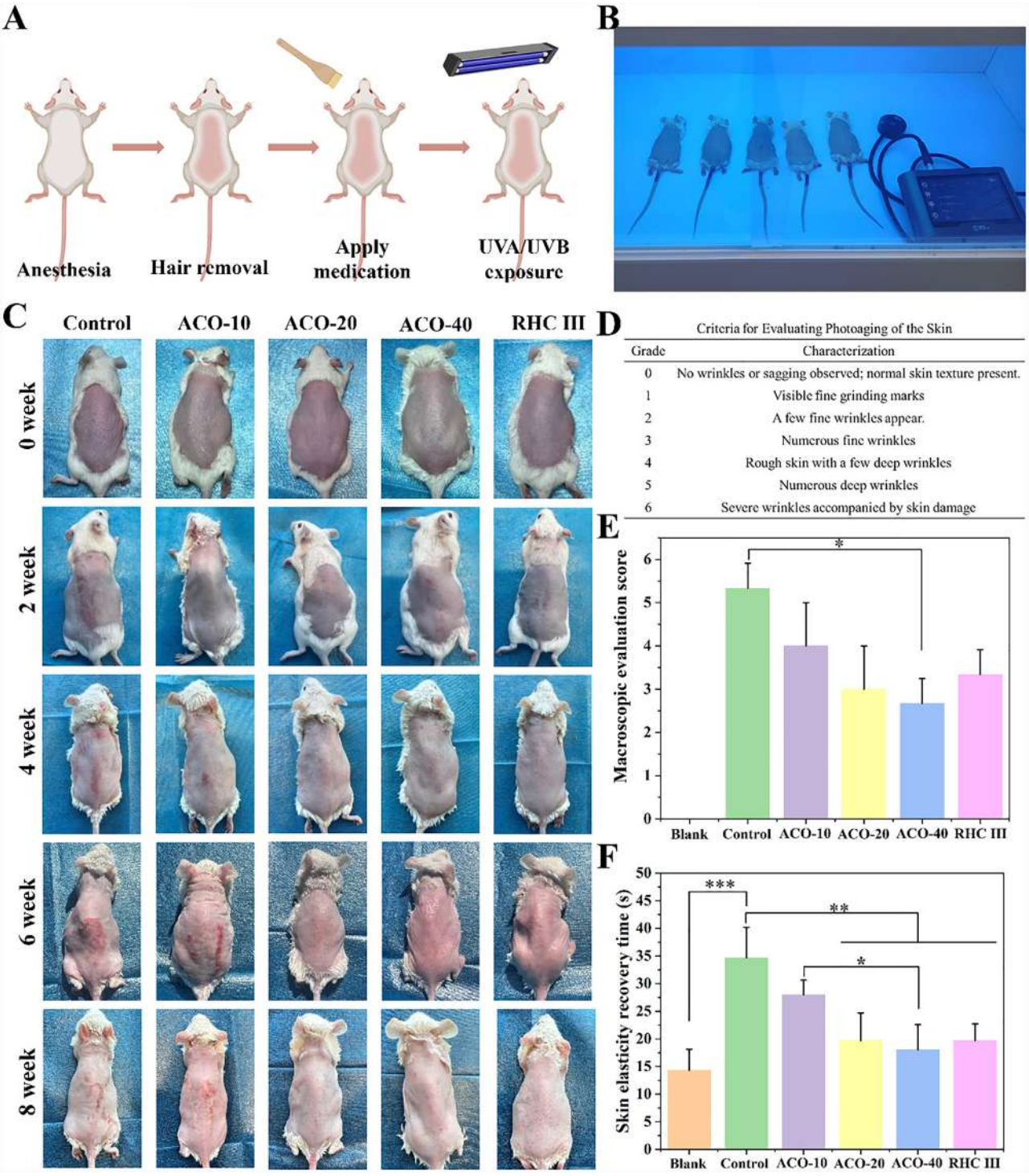

Fig. 4. Macroscopic evaluation of the anti-photoaging effects of ACO in mouse skin. (A) Schematic diagram of the mouse photoaging model establishment. (B) Photograph of mice exposed to UVA/UVB irradiation. (C) Gross appearance changes of mice at different time points after UV irradiation. (D) Scoring criteria table for macroscopic assessment of skin photoaging. (E) Macroscopic photoaging scores of mouse skin among different treatment groups after UV irradiation (n = 5). (F) Statistical analysis of skin retraction time in the dorsal skin of mice (n = 5). $^{*}p < 0.05$, $^{**}p < 0.01$, $^{***}p < 0.001$.

and structure of the elastic fibers became increasingly similar to those of the blank group, with the ACO-40 group showing the closest similarity. These results indicate that ACO can effectively maintain the structural integrity of elastic fibers, thereby helping preserve skin elasticity.

In summary, ACO effectively delays the progression of skin photoaging, with observed benefits including maintenance of elastic fiber structural integrity, promotion of collagen synthesis coupled with inhibition of its degradation, and attenuation of inflammatory responses, highlighting its promising anti-photoaging potential.

3.9. Effect of ACO on oxidant-antioxidant homeostasis in photoaging mice

Chronic UV exposure disrupts the skin's redox balance by triggering excessive ROS generation [7]. Thus, the antioxidant capacity of the skin

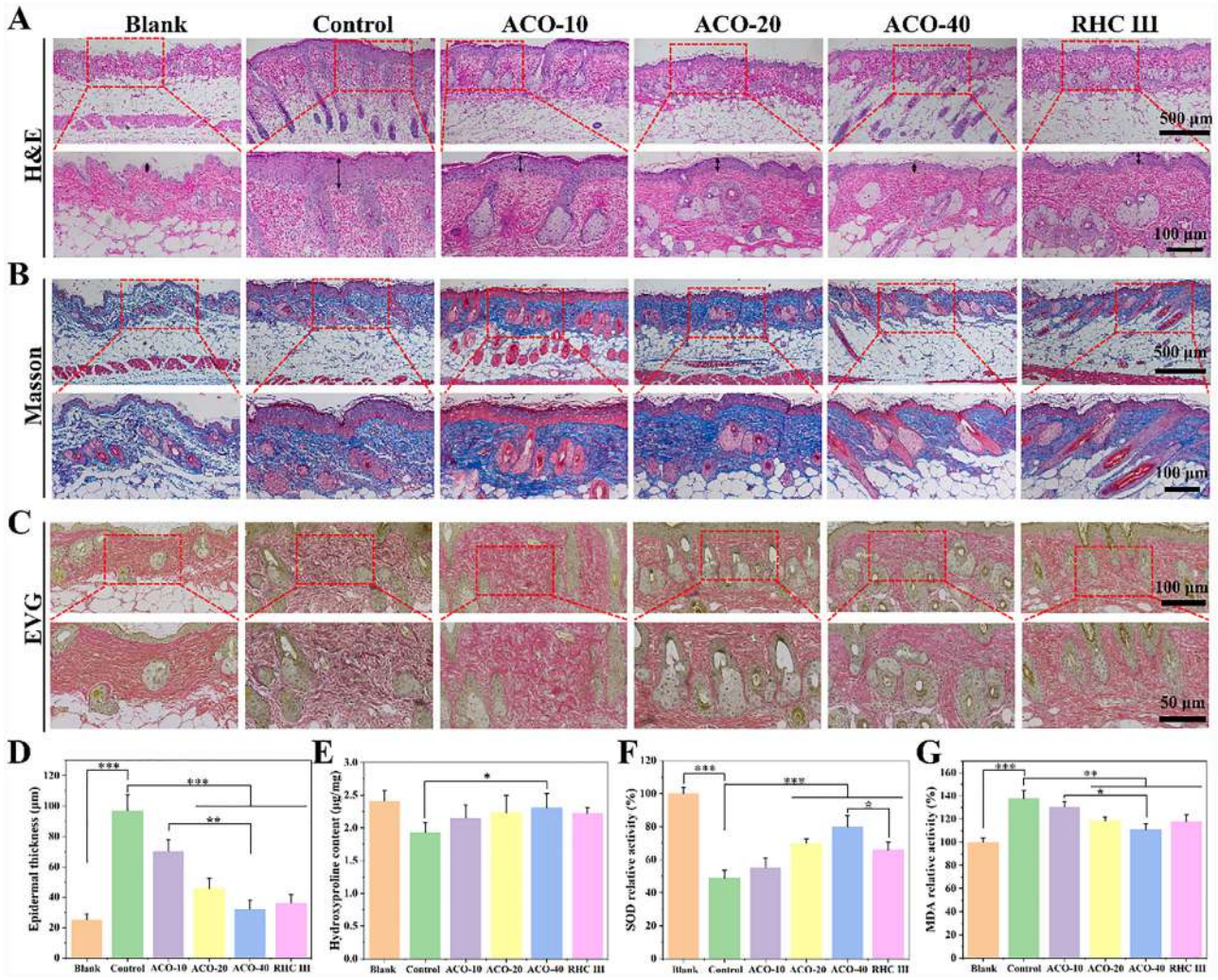

Fig. 5. Effects of ACO on histological structure and oxidant-antioxidant homeostasis in photoaging mice. (A) Representative H&E staining images of dorsal skin tissue. (B) Representative Masson's trichrome staining images of dorsal skin tissue. (C) Representative EVG staining images of dorsal skin tissue. (D) Epidermal thickness measurements among different groups after UV irradiation (n = 5). (E) HYP content in skin tissues from different groups after UV irradiation (n = 5). (F) SOD levels in different groups after UV irradiation (n = 5). (G) MDA levels in different groups after UV irradiation (n = 5). $^{*}p < 0.05$, $^{**}p < 0.01$, $^{***}p < 0.001$.

can be evaluated by detecting the levels of SOD and MDA. As shown in Fig. 5F and 5G, with the blank group set as 100%, the SOD content in the model control group decreased significantly to 48.86%, while the MDA content increased markedly to 137.76%. These results indicate that UV irradiation reduces SOD levels and increases MDA content in mouse skin tissue, leading to increased skin oxidative stress. Compared with the model control group, all ACO treatment groups and the RHT-III group showed increased SOD content and decreased MDA levels. Among them, the ACO-40 group exhibited a more significant increase in SOD content compared with the ACO-10 and ACO-20 groups ($p < 0.05$), along with a further reduction in MDA content, demonstrating a dose-dependent improvement trend. SOD is a crucial antioxidant enzyme *in vivo* [41]. By increasing the SOD content in skin cells, ACO enhances the ability to scavenge ROS. On the other hand, MDA, as an end product of lipid peroxidation, directly reflects the degree of oxidative damage to the cell membrane system [42]. The significant reduction of MDA levels in skin tissue by ACO indicates its ability to effectively inhibit UV-induced membrane lipid peroxidation, thereby preserving the integrity of the cell membrane and preventing cellular dysfunction. In summary, through the synergistic regulation of these two key oxidative stress indicators (SOD and MDA), ACO helps restore the oxidant-antioxidant balance disrupted by UV irradiation, demonstrating considerable potential in delaying skin photoaging.

4. Discussion

From the perspective of skin photoprotection mechanisms, the dual effects of ACO in promoting keratinocyte proliferation and migration hold important physiological significance. Firstly, epidermal thickness, particularly the integrity of the stratum corneum, serves as the primary physical barrier against UV irradiation [43]. By augmenting the proliferation and migration of basal keratinocytes, the epidermal renewal process is accelerated, leading to an increased number of cell layers and a consequent enhancement of overall epidermal thickness [44]. This structural adaptation effectively scatters and absorbs a greater proportion of UV irradiation, thereby mitigating photodamage at its source. Secondly, acute UV exposure often induces keratinocyte apoptosis, disrupting epidermal continuity [44]. Enhancing their proliferative and migratory capacity facilitates the rapid repair of UV-induced epithelial defects, accelerates the restoration of the skin barrier, reduces transepidermal water loss, and blocks the intrusion of external harmful agents, thereby establishing a stable internal microenvironment conducive to tissue repair [45]. Furthermore, keratinocytes with heightened proliferative and migratory activity typically exhibit superior metabolic and functional states [46]. This not only enhances the cell's intrinsic capacity for DNA damage repair and antioxidant defense but also promotes the synthesis and secretion of endogenous defense molecules, collectively

strengthening the epidermis' overall resilience and self-repair potential [47]. In summary, by synergistically promoting keratinocyte proliferation and migration, ACO not only reinforces the skin's passive defensive capabilities but also confers active biological functions for damage repair, thereby constituting a dynamic, proactive, and efficient photoprotection system for skin tissue.

In cellular senescence models, ACO exerts comprehensive protective effects against UV-induced damage by multi-pathway regulation of dermal fibroblast function. On one hand, ACO directly promotes the synthesis and secretion of Col-I, Col-III, and elastin in fibroblasts. These proteins are core components of the dermal structural scaffold and elastic network. Enhancing their synthesis effectively compensates for the ECM loss caused by UV irradiation, helping to maintain skin thickness, firmness, and elasticity, thereby strengthening the skin's physical barrier function and structural support capacity against UV exposure [48]. On the other hand, ACO downregulates the expression of MMPs (such as MMP-1), reducing their degradation of collagen and elastin. This inhibitory effect synergizes with the promotion of synthesis to collectively maintain ECM metabolic balance, effectively preserving the integrity of the existing dermal structure and delaying wrinkle formation and skin laxity [48]. Compared with VE (a potent antioxidant), high concentrations of ACO exhibit comparable effects in promoting matrix synthesis and inhibiting degradation, suggesting that ACO may inhibit UV-induced oxidative stress and DNA damage, delay fibroblast senescence, and maintain their normal proliferation and physiological functions, thereby ensuring the stability and self-renewal capacity of the dermal structure at the source [49]. In summary, ACO exerts multi-pathway and multi-targeted anti-photoaging effects by maintaining cellular functional homeostasis, promoting the synthesis of structural proteins, and inhibiting their degradation.

Based on *in vitro* experimental results, this study further validated the ameliorative effect of ACO on UV-induced skin damage by establishing a mouse photoaging model. Macroscopically, ACO intervention exhibited a dose-dependent reduction in desquamation, wrinkling, hyperpigmentation, and decreased elasticity on the backs of model mice, with the ACO-40 high-dose group showing the most pronounced effects, exhibiting skin conditions approaching those of normal mice. Histological analysis revealed that ACO significantly suppressed UV-induced abnormal epidermal thickening, protected the integrity of collagen and elastic fibers, and prevented their degradation, breakage, and curling. Concurrently, ACO markedly elevated hydroxyproline content in skin and regulated oxidative-antioxidant balance, manifested as increased SOD activity and reduced MDA levels. In summary, ACO effectively delays the progression of photoaging, with observed benefits including protecting extracellular matrix structure, promoting collagen homeostasis, and alleviating oxidative stress, demonstrating significant potential as an anti-photoaging active ingredient. Research on the dermatological effects of ACO is still in its infancy [14]. Previous studies have made preliminary progress in anti-skin aging, amelioration of oxidative damage in vascular endothelial cells, and elucidation of its protein composition [15–17,19]. Building upon these findings, the present study systematically validated the anti-photoaging effects of ACO in both skin fibroblasts and photoaged animal models, extending the functional research of ACO from traditional hematopoiesis and hemostasis to skin photoprotection.

Based on the phenotypic data described above, we further explored the potential molecular mechanisms underlying the observed effects. Although the activation status of specific signaling pathways was not directly assessed in this study, the observed phenotypic changes, including increased collagen synthesis, reduced MMP expression, and enhanced antioxidant capacity, provide indirect evidence for the involvement of multiple well-established photoaging-related pathways. Regarding the TGF-β/Smad pathway, this signaling cascade is a master regulator of type I and type III collagen expression in dermal fibroblasts [50]. UV irradiation suppresses TGF-β receptor activation and Smad2/3 phosphorylation, thereby downregulating collagen production [51]. Our finding that ACO treatment significantly elevated Col-I and Col-III levels and increased hydroxyproline content in UV-exposed skin suggests that ACO may counteract UV-induced suppression of TGF-β/Smad signaling (Fig. 3D, 3E, and 5E). However, this inference requires direct verification through measurement of TGF-β1, phosphorylated Smad2/3, and Smad4 expression. With respect to the MAPK/AP-1 pathway, the MAPK cascade (including ERK, JNK, and p38) is activated by UV-induced oxidative stress, which in turn activates AP-1 (c-Fos/c-Jun) and upregulates MMPs, leading to degradation of collagen and elastin [52,53]. Our results demonstrated that ACO significantly inhibited MMP-1 expression in both UV-induced senescent fibroblasts and UV-irradiated mouse skin (Fig. 3G), suggesting that ACO may suppress UV-induced MAPK/AP-1 pathway activation and thereby mitigate extracellular matrix degradation. Regarding the Nrf2/ARE pathway, this pathway serves as a central hub for antioxidant defense, regulating the expression of HO-1, NQO1, SOD, and other detoxifying enzymes [54]. UV irradiation impairs Nrf2 nuclear translocation, resulting in diminished antioxidant capacity [55]. Our data showed that ACO treatment increased SOD activity and decreased MDA levels in UV-exposed skin (Fig. 5F and 5G), indicating enhanced antioxidant defense potentially involving Nrf2 pathway activation. However, this hypothesis requires confirmation through direct measurement of nuclear Nrf2 accumulation and HO-1/NQO1 expression. Collectively, these correlative observations are consistent with the hypothesis that ACO may modulate the TGF-β/Smad, MAPK/AP-1, and Nrf2/ARE pathways.

From an application perspective, as a natural-derived complex, ACO may offer superior safety and tolerability compared with chemically synthesized anti-photoaging agents [10,13]. In the present study, ACO was systematically compared with VE and RHT-III. VE, a classic lipophilic antioxidant, exhibits well-defined free radical scavenging activity and favorable skin permeability, and has been extensively employed as a positive control in anti-photoaging research [22,23]. However, VE suffers from poor stability, is prone to oxidative inactivation, and may cause skin irritation upon prolonged high-concentration use [56]. In contrast, as a complex polypeptide system, ACO not only directly scavenges free radicals through its peptide moieties but also exerts synergistic effects by activating endogenous antioxidant defense systems (e.g., SOD and CAT) [19]. This multi-target antioxidant mode confers a potential advantage over single-molecule antioxidants. RHT-III, as an exogenous collagen supplement, directly supplies collagen synthesis substrates to the skin, replenishing collagen depleted by photoaging [24,25]. In contrast, ACO acts through a dual mechanism: it directly provides collagen peptide substrates while simultaneously reducing endogenous collagen degradation via MMP-1 inhibition, thereby more comprehensively maintaining collagen metabolic homeostasis. This supplementation plus protection dual mode represents a unique advantage of ACO over simple collagen supplements. Within the experimental concentration range (0.156-20 mg/mL), ACO exhibited no cytotoxicity and effectively promoted cell proliferation and migration even at lower concentrations. ACO offers advantages including broad availability, mature preparation technology, and proven safety for both oral and topical administration. These findings provide experimental evidence for the development of ACO as a functional skincare ingredient or photoprotective agent, and open new avenues for the modern application of the traditional Chinese medicine ACO in skin health.

Nevertheless, several limitations of this study should be acknowledged, primarily in two aspects. At the mechanistic level, although we observed regulatory effects of ACO on collagen synthesis, MMP-1 expression, and antioxidant enzyme activities, and speculated on the potential involvement of TGF-β/Smad, MAPK/AP-1, and Nrf2/ARE pathways based on literature correlations, all mechanistic inferences are derived from phenotypic endpoints (collagen and elastin content, MMP-1 expression levels, SOD and MDA activities), without direct verification of the activation status of these signaling pathways (e.g., Smad2/3 phosphorylation, AP-1 activation, Nrf2 nuclear translocation). Future studies employing Western blotting, immunohistochemistry, and pathway-specific interventions are warranted to elucidate the causal relation-

ships between ACO and specific signaling pathways. At the product translation level, as a natural-derived complex, ACO possesses a chemically complex composition, and its anti-photoaging activity may arise from synergistic effects among multiple peptides, glycosaminoglycans, and trace elements, rather than from a single component. This "multi-component, multi-target" feature constitutes both a unique advantage as a natural product and a challenge for precise standardization of active ingredients, accurate mechanistic dissection, and batch-to-batch consistency control. Therefore, establishing a full-chain standardization system encompassing raw material traceability, extraction processes, and quality control is a core prerequisite for promoting ACO industrialization. Meanwhile, activity-guided fractionation strategies will facilitate the identification of specific active peptides or protein components that play key roles in ACO, thereby enabling the discovery of more selective and potent lead compounds. In addition, although this study preliminarily confirmed the safety of topical ACO administration, the potential long-term effects on skin barrier function, microecological balance, and systemic absorption still require evaluation through chronic toxicity studies and clinical observation. Overall, the current findings provide reliable data supporting the phenotypic effects of ACO against photoaging and offer testable scientific hypotheses for future mechanistic investigations.

5. Conclusions

This study systematically elucidates the multiple mechanisms and potent efficacy of ACO in protecting against skin photoaging. At the cellular level, ACO exhibits favorable biocompatibility and significantly promotes the proliferation and migration of keratinocytes. These effects help establish an effective physical defense system for the skin by enhancing the epidermal barrier function and accelerating damage repair. In terms of delaying cellular senescence, ACO effectively inhibits UV-induced oxidative stress damage and maintains the integrity and function of the dermal structure by promoting the synthesis of Col-I, Col-III, and elastin. In animal experiments, ACO demonstrates a clear dose-dependent effect in mitigating skin photoaging. By increasing SOD content and reducing MDA levels, it effectively restores oxidant-antioxidant balance and alleviates lipid peroxidation damage. Collectively, through multiple mechanisms, including promoting epidermal cell proliferation and migration, delaying cellular senescence, regulating ECM metabolic homeostasis, and maintaining redox balance, ACO constructs a comprehensive photoaging protection system, showing promising application prospects in the prevention and amelioration of skin photoaging.

Declaration of competing interest

This study used Dong'e Ejiao as an experimental sample, which was provided by Dong'e Ejiao Co., Ltd. The company also provided research funding. Several authors (Xiao Xie, Zhijie Chen, Cong Li, Jianling Zhang,) are employees of Dong'e Ejiao Co., Ltd. Notwithstanding these relationships, all authors declare that the study design, execution, data collection, analysis, interpretation, and manuscript writing were conducted independently and objectively, without undue influence from the company's commercial interests. The manuscript was not reviewed or approved by the company prior to submission, and the authors assume full responsibility for the integrity and accuracy of the study findings. Apart from the employment and funding relationships described above, the authors declare that there are no other known competing financial interests or personal relationships that could influence the work reported in this paper.

CRediT authorship contribution statement

Xiao Xie: Writing – review & editing, Supervision, Software, Resources, Methodology, Conceptualization. **Zhijie Chen:** Visualization, Resources, Methodology, Data curation, Conceptualization. **Zesong Zhang:** Writing – review & editing, Investigation, Funding acquisition, Formal analysis, Data curation, Conceptualization. **Zailin Chen:** Writing – review & editing, Investigation, Data curation, Conceptualization. **Cong Li:** Resources, Project administration, Investigation, Conceptualization. **Jianling Zhang:** Resources, Project administration, Formal analysis, Data curation. **Jiahao Yang:** Visualization, Validation, Methodology. **Zhihui Lu:** Validation, Supervision, Project administration. **Lei Jia:** Visualization, Validation, Resources, Project administration. **Meimei Fu:** Writing – review & editing, Writing – original draft, Methodology, Investigation, Formal analysis, Data curation, Conceptualization. **Jinshan Guo:** Writing – review & editing, Resources, Project administration, Methodology, Investigation, Conceptualization.

Data availability: The data that support the findings of this study are available from the corresponding author.

Acknowledgements

This work was supported by an industry-sponsored project (DEEJ-YB-2024-10-190) with Dong'e Ejiao Health Products Co. Ltd. We are grateful to Prof. Sheng Xiong of Jinan University for kindly providing the recombinant humanized type III collagen (RHT-III) used in this study.

Supplementary materials

Supplementary material associated with this article can be found, in the online version, at doi:10.1016/j.engreg.2026.07.001.

References

[1] C. He, Z. Wang, Z. Jiang, Y. Zhou, X. Chen, J. Zhang, B. Wang, Q. Wang, T. Wu, C. Li, Z. Jian, Microneedles combining delivery of hUMSC-derived exosomes and EGCG mitigate UV-induced skin damage, J. Nanobiotechnol. 23 (1) (2025) 643, doi:10.1186/s12951-025-03735-x.
[2] F. Lu, J. Zhong, Q. Zhou, Y. Yu, M. Liang, Y. Yuan, A. Xie, J. Cheng, P. Shu, J. Hao, Okanin attenuates mitochondrial dysfunction and apoptosis in UVA-induced HaCaT cells by mitophagy through SIRT3 pathway, Antioxidants 14 (9) (2025) 1040, doi:10.3390/antiox14091040.
[3] X. Yao, H. Li, L. Chen, L.P. Tan, UV-induced senescence of human dermal fibroblasts restrained by low-stiffness matrix by inhibiting NF-κb activation, Eng. Regen. 3 (4) (2022) 365–373, doi:10.1016/j.engreg.2022.08.002.
[4] F. Shang, Y. Qu, Z. Wang, L. Dong, A. Li, D. Zhang, S. Gong, Y. Gao, Q. Bai, L. Ming, L. Shao, Activation of Nrf2 with natural flavonoids and mesenchymal stromal/stem cells: Mechanisms and therapeutic potential for inflammatory diseases, Stem Cell Res. Ther. 17 (122) (2026), doi:10.1186/s13287-026-04925-6.
[5] C. Liang, Y. Yi, J. Li, S. Aghayants, X. Chen, W. Cao, Q. Zhang, Unveiling exosomes in combating skin aging: insights into resources, mechanisms and challenges, Stem Cell Res. Ther. 16 (1) (2025) 474, doi:10.1186/s13287-025-04620-y.
[6] M. Kaltchenko, A. Chien, Photoaging: current concepts on molecular mechanisms, prevention, and treatment, Am. J. Clin. Dermatol. 26 (3) (2025) 321–344, doi:10.1007/s40257-025-00933-z.
[7] M. Tanveer, H. Rashid, S. Tasduq, Molecular basis of skin photoaging and therapeutic interventions by plant-derived natural product ingredients: a comprehensive review, Heliyon 9 (3) (2023) e13580, doi:10.1016/j.heliyon.2023.e13580.
[8] P. Maunjumpon, O. Thamsermsang, U. Panich, Mitigating PM2.5-induced skin injury and aging: botanical strategies targeting redox and inflammatory pathways, Redox Rep. 31 (1) (2026) 2629079, doi:10.1080/13510002.2026.2629079.
[9] J. Wang, M. Yuan, Q. Li, C. Shen, X. Zhang, C. Zhu, Q. Cen, Combined protection against UVB-induced photoaging by oleuropein, hydroxytyrosol, and verbascoside through modulation of inflammation, oxidative stress, and collagen homeostasis, Sci. Rep. 15 (1) (2025) 41008, doi:10.1038/s41598-025-24845-4.
[10] X. Yu, L. Kong, B. Wang, C. Zhai, Y. Lao, L. Zhang, Y. Gao, B. Zhao, Asini Corii Colla (Ejiao) as a health-care food and traditional Chinese medicine: a review of its chemical composition, pharmacological activity, quality control, modern applications, J. Funct. Foods 125 (2025) 106678, doi:10.1016/j.jff.2025.106678.
[11] Y. Mo, X. He, P. Shi, Y. Ning, M. Zhou, H. Cui, T. Zhang, Hematopoietic effects of Fufang E'jiao Jiang revealed by microbiome, metabolome and transcriptome analyses: a multi-omics strategy, Front. Immunol. 16 (2025) 1561477, doi:10.3389/fimmu.2025.1561477.
[12] L. Zhang, Z. Xu, T. Jiang, J. Zhang, P. Huang, J. Tan, G. Chen, M. Yuan, Z. Li, H. Liu, D. Gao, L. Xiao, H. Feng, J. Xu, H. Xu, Efficacy and safety of Ejiao (Asini Corii Colla) in women with blood deficient symptoms: a randomized, double-blind, and placebo-controlled clinical trial, Front. Pharmacol. 12 (2021) 718154, doi:10.3389/fphar.2021.718154.
[13] Y. Wang, G. Chen, Q. Wang, Z. Zhou, W. Zhao, S. Wong, T. Wang, K. Chin, A comprehensive review of traditional Chinese medicine Ejiao (Colla Corii Asini): chemical composition, quality control, and pharmacological actions, Nat. Prod. Commun. 20 (4) (2025), doi:10.1177/1934578x251335424.

[14] F. Wu, X. Xie, W. Ru, X. Guo, L. Meng, J. Zhang, X. Liu, Y. Pan, A deep dive into the potential antiaging effects of Colla Corii Asini on the skin: a comparative study, J. Cosmet. Dermatol. 24 (3) (2025) e70080, doi:10.1111/jocd.70080.
[15] C. Li, M. Ji, L. Meng, X. Ma, J. Zhang, Y. Yuan, Q. Yu, L. Fan, Study on anti-skin aging effect of different polar solvent extracts of Colla Corii Asini and Ejiao cake, Food Ferment. Indust. 51 (17) (2025) 82–92, doi:10.13995/j.cnki.11-1802/ts.041370.
[16] H. Tie, X. Xie, Z. Zhang, J. Zhang, L. Xu, H. Ruan, T. Wu, H. Zhang, E'jiao and Cubilose formula induced antioxidant activity and improved collagen expression of Human skin fibroblasts during oxidation damage, J. Cosmet. Dermatol. 24 (2025) e16604, doi:10.1111/jocd.16604.
[17] E. Chuo, L. Meng, C. Li, X. Ma, H. Wu, J. Zhang, J. Zheng, L. Fan, Effects of Colla Corii Asini (Ejiao) cake extract on the metabolism of mouse melanoma cells, Food Sci. Technol. 50 (4) (2025) 222–230, doi:10.13995/j.cnki.11-1802/ts.041370.
[18] L. Xiao, F. Liao, Y. Fan, N. Miwa, Enzyme-digested Colla Corii Asini (E'jiao) accelerates wound healing and prevents ultraviolet A-induced collagen synthesis decline and wrinkle formation in three-dimensional skin equivalents, Hum. Cell 33 (4) (2020) 1056–1067, doi:10.1007/s13577-020-00405-y.
[19] X. Xie, C. Li, J. Zhang, Z. Chen, C. Tao, M. Fu, H. You, J. Guo, Proteomic analysis and the antioxidant activity evaluation of Asini Corii Colla powder based on liquid chromatography-tandem mass spectrometry technology, Chin. J. Appl. Chem. 43 (3) (2026) 396–410, doi:10.19894/j.issn.1000-0518.250344.
[20] M. Fu, Y. Zhao, Y. Wang, Y. Li, M. Wu, Q. Liu, Z. Hou, Z. Lu, K. Wu, J. Guo, On-demand removable self-healing and pH-responsive europium-releasing adhesive dressing enables inflammatory microenvironment modulation and angiogenesis for diabetic wound healing, Small 19 (3) (2023) e2205489, doi:10.1002/smll.202205489.
[21] M. Fu, Q. Xiang, Z. Huang, W. Luo, Z. Fang, J. Li, Y. Li, Z. Xia, Y. Huang, Y. Zhao, W. Liao, J. Guo, Photo-cross-linked and photothermal Flammulina Velutipes polysaccharide hydrogel loaded with caffeic acid-copper nanozyme for diabetic wound healing, ACS Appl. Mater. Interf. 17 (38) (2025) 53145–53167, doi:10.1021/acsami.5c11453.
[22] Q. Jiang, Natural forms of vitamin E: metabolism, antioxidant, and anti-inflammatory activities and their role in disease prevention and therapy, Free Radical Biol. Med. 72 (2014) 76–90, doi:10.1016/j.freeradbiomed.2014.03.035.
[23] G. Burton, M. Traber, Vitamin E: antioxidant activity, biokinetics, and bioavailability, Annu. Rev. Nutr. 10 (1990) 357–382, doi:10.1146/annurev.nu.10.070190.002041.
[24] S. Ye, B. Chen, L. Jeevithan, H. Yang, Y. Kong, X. Diao, W. Wu, Recombinant humanized collagen enhances secreted protein levels of fibroblasts and facilitates rats' skin basement membrane reinforcement, J. Funct. Biomater. 16 (2) (2025) 47, doi:10.3390/jfb16020047.
[25] A. Rahman, R. Rehmani, D.G. Pirvu, S.M. Huang, S. Puri, M. Arcos, Unlocking the therapeutic potential of marine collagen: a scientific exploration for delaying skin aging, Mar. Drugs 22 (4) (2024) 159, doi:10.3390/md22040159.
[26] M. Fu, Y. Li, Y. Zhao, Y. Zhu, Z. Fang, Z. Huang, W. Luo, X. Huang, J. Li, Z. Hu, K. Wu, J. Guo, Janus adhesive dressing with macro/micro dual design enabling sequential microenvironment regulation for scarless wound healing, Adv. Fiber Mater. 8 (1) (2026) 262–288, doi:10.1007/s42765-025-00620-y.
[27] V.T. Natarajan, P. Ganju, A. Ramkumar, R. Grover, R.S. Gokhale, Multifaceted pathways protect human skin from UV radiation, Nat. Chem. Biol. 10 (7) (2014) 542–551, doi:10.1038/nchembio.1548.
[28] M. Wu, Y. Zhao, M. Tao, M. Fu, Y. Wang, Q. Liu, Z. Lu, J. Guo, Malate-based biodegradable scaffolds activate cellular energetic metabolism for accelerated woundhealing, ACS Appl. Mater. Interf. 15 (44) (2023) 50836–50853, doi:10.1021/acsami.3c09394.
[29] J. Shin, J.H. Kim, E.K. Kim, Repeated exposure of human fibroblasts to UVR induces secretion of stem cell factor and senescence, J. Eur. Acad. Dermatol. 26 (12) (2012) 1577–1580, doi:10.1111/j.1468-3083.2011.04223.x.
[30] X. Lin, A.M. Filppula, L. Shang, H. Zhang, D. Wang, Microcarriers encapsulating COL1A1 mRNA-loaded nanovesicles for skin photoaging treatment, Mater. Today Bio. 38 (2026) 103126, doi:10.1016/j.mtbio.2026.103126.
[31] J. Zhou, M. Guo, Y. Peng, W. Xu, X. Hao, Y. Tang, T. Tang, J. Wu, D. Xiang, Beta vulgaris-derived exosome-like nanovesicles mitigate photoaging by attenuating oxidative stress and promoting collagen biosynthesis, Colloids Surf. B 261 (2026) 115412, doi:10.1016/j.colsurfb.2025.115412.
[32] F. Debacq-Chainiaux, J.D. Erusalimsky, J. Campisi, O. Toussaint, Protocols to detect senescence-associated beta-galactosidase (SA-betagal) activity, a biomarker of senescent cells in culture and in vivo, Nat. Protoc. 4 (12) (2009) 1798–1806, doi:10.1038/nprot.2009.191.
[33] E. Mavrogonatou, A. Papadopoulou, H. Pratsinis, D. Kletsas, Senescence-associated alterations in the extracellular matrix: deciphering their role in the regulation of cellular function, Am. J. Physiol. Cell Physiol. 325 (3) (2023) C633–C647, doi:10.1152/ajpcell.00178.2023.
[34] O. Bar, S. Valiukevičienė, Skin aging and type I collagen: a systematic review of interventions with potential collagen-related effects, Cosmetics 12 (4) (2025) 129, doi:10.3390/cosmetics12040129.
[35] C. Lovell, K. Smolenski, V. Duance, N. Light, S. Young, M. Dyson, Type I and III collagen content and fibre distribution in normal human skin during ageing, Brit. J. Dermatol. 117 (4) (1987) 419–428, doi:10.1111/j.1365-2133.1987.tb04921.x.
[36] J. Lee, Y. Kim, J. Seo, C. Choi, J. Hwang, B. Lee, I. Chang, J. Chung, Loss of elastic fibers causes skin wrinkles in sun-damaged human skin, J. Dermatol. Sci. 50 (2) (2008) 99–107, doi:10.1016/j.jdermsci.2007.11.010.
[37] S. Shapiro, R. Senior, Matrix metalloproteinases: matrix degradation and more, Am. J. Respir. Cell Mol. Biol. 20 (6) (1999) 1100–1102, doi:10.1165/ajrcmb.20.6.f151.
[38] R. Agrawal, I. Kaur, Inhibitory effect of encapsulated curcumin on ultraviolet-induced photoaging in mice, Rejuv. Res. 13 (4) (2010) 397–410, doi:10.1089/rej.2009.0906.
[39] Y. Liang, Y. Sun, X. Li, L. Yan, J. Wang, J. Hu, H. Yu, H. Xiao, H. Chen, Z. Sun, J. Cai, X. Feng, C. Xiong, J. He, The optimal concentration of topical hydroxycamptothecin in preventing intraarticular scar adhesion, Sci. Rep. 4 (2014) 4621, doi:10.1038/srep04621.
[40] T. Abe, A. Hashiguchi, K. Yamazaki, H. Ebinuma, H. Saito, H. Kumada, N. Izumi, N. Masaki, M. Sakamoto, Quantification of collagen and elastic fibers using whole-slide images of liver biopsy specimens, Pathol. Int. 63 (6) (2013) 305–310, doi:10.1111/pin.12064.
[41] M. Islam, A. Rauf, F. Fahad, T. Emran, S. Mitra, A. Olatunde, M. Shariati, M. Rebezov, K. Rengasamy, M. Mubarak, Superoxide dismutase: an updated review on its health benefits and industrial applications, Crit. Rev. Food Sci. Nutr. 62 (26) (2022) 7282–7300, doi:10.1080/10408398.2021.1913400.
[42] J. Ding, B. Gao, Z. Sang, Z. Dai, Z. Chen, X. Mei, Promoting spinal cord injury repair by using ZnO@MOFs nanozymes functionalized hydrogel through the ROS microenvironment regulating pathway, Regener. Biomater. 12 (2025) rbaf095, doi:10.1093/rb/rbaf095.
[43] J. Orazio, S. Jarrett, A. Amaro-Ortiz, T. Scott, UV radiation and the skin, Int. J. Mol. Sci. 14 (6) (2013) 12222–12248, doi:10.3390/ijms140612222.
[44] C. Lee, S. Wu, C. Hong, H. Yu, Y. Wei, Molecular mechanisms of UV-induced apoptosis and its effects on skin residential cells: the implication in UV-based phototherapy, Int. J. Mol. Sci. 14 (3) (2013) 6414–6435, doi:10.3390/ijms14036414.
[45] B. Berman, C. Cockerell, Pathobiology of actinic keratosis: ultraviolet-dependent keratinocyte proliferation, J. Am. Acad. Dermatol. 68 (2013) S10–S19, doi:10.1016/j.jaad.2012.09.053.
[46] J. Zhu, C. Thompson, Metabolic regulation of cell growth and proliferation, Nat. Rev. Mol. Cell Biol. 20 (7) (2019) 436–450, doi:10.1038/s41580-019-0123-5.
[47] M. Piipponen, D. Li, N. Landén, The immune functions of keratinocytes in skin wound healing, Int. J. Mol. Sci. 21 (22) (2020) 8790, doi:10.3390/ijms21228790.
[48] S. Wang, F. Li, X. Feng, M. Feng, X. Niu, X. Jiang, W. Chen, R. Bai, Promoting collagen synthesis: a viable strategy to combat skin ageing, J. Enzyme Inhib. Med. Chem. 40 (1) (2025) 2488821, doi:10.1080/14756366.2025.2488821.
[49] L. Xiao, F. Liao, R. Ide, T. Horie, Y. Fan, C. Saiki, N. Miwa, Enzyme-digested Colla Corii Asini (E'jiao) prevents hydrogen peroxide-induced cell death and accelerates amyloid beta clearance in neuronal-like PC12 cells, Neur. Regen. Res. 15 (12) (2020) 2270–2277, doi:10.4103/1673-5374.285000.
[50] T. Yang, H. Xu, The critical role of LRG1 in pathological fibrosis, J. Mol. Med. 103 (11-12) (2025) 1317–1332, doi:10.1007/s00109-025-02596-z.
[51] K. Han, H. Choi, C. Won, J. Chung, K. Cho, H. Eun, K. Kim, Alteration of the TGF-beta/SMAD pathway in intrinsically and UV-induced skin aging, Mech. Age. Dev. 126 (5) (2005) 560–567, doi:10.1016/j.mad.2004.11.006.
[52] J. Oh, J. Kim, F. Karadeniz, H. Kim, S. Park, Y. Seo, C. Kong, Santamarine shows anti-photoaging properties via inhibition of MAPK/AP-1 and stimulation of TGF-β/smad signaling in UVA-irradiated HDFs, Molecules 26 (12) (2021) 3585, doi:10.3390/molecules26123585.
[53] Y. He, S. Yin, R. Xu, Y. Zhao, Y. Du, Z. Duan, D. Fan, Recombinant type XVII collagen inhibits EGFR/MAPK/AP-1 and activates TGF-β/smad signaling to enhance collagen secretion and reduce photoaging, Cosmetics 12 (2) (2025) 59, doi:10.3390/cosmetics12020059.
[54] Z. Sun, Y. Zheng, T. Wang, J. Zhang, J. Li, Z. Wu, F. Zhang, T. Gao, L. Yu, X. Xu, H. Qian, Y. Tan, Aloe vera gel and rind-derived nanoparticles mitigate skin photoaging via activation of Nrf2/ARE pathway, Int. J. Nanomed. Volume 20 (2025) 4051–4067, doi:10.2147/ijn.S510352.
[55] C. Liu, Y. Chen, I.E. Kochevar, U.V. Jurkunas, Decreased DJ-1 leads to impaired Nrf2-regulated antioxidant defense and increased UV-A-induced apoptosis in corneal endothelial cells, Invest. Ophthalmol. Vis. Sci. 55 (9) (2014) 5551, doi:10.1167/iovs.14-14580.
[56] S. Dinić, J. Arambašić Jovanović, A. Uskoković, M. Mihailović, N. Grdović, A. Tolić, J. Rajić, M. Đorđević, M. Vidaković, Oxidative stress-mediated beta cell death and dysfunction as a target for diabetes management, Front. Endocrinol. 13 (2022) 1006376, doi:10.3389/fendo.2022.1006376.